

COMPARISON OF TURBULENT BOUNDARY LAYERS AND CHANNELS FROM  
DIRECT NUMERICAL SIMULATIONJavier Jiménez<sup>†,§,1</sup>, Sergio Hoyas<sup>†,‡</sup>, Mark P. Simens<sup>†</sup> and Yoshinori Mizuno<sup>†</sup><sup>†</sup> School of Aeronautics, Universidad Politécnica de Madrid  
28040 Madrid, Spain<sup>§</sup> Centre for Turbulence Research, Stanford University  
Stanford CA 94305<sup>‡</sup> CMT Motores Térmicos, Univ. Politécnica de Valencia  
E-46022 Valencia, Spain

## ABSTRACT

A new simulation of the zero-pressure-gradient turbulent boundary layer is discussed, in the range  $Re_\theta = 620 - 2140$ . It is first shown that the initial several hundred momentum thicknesses have to be discarded due to contamination from the synthetic turbulent inflow, and this is traced to the long lifetimes of the largest eddies.

Beyond the inflow region, the results agree well with previous simulations and with experiments, and are compared to those of turbulent channels in the same range of Reynolds numbers. It is found that the transverse velocities and the pressure fluctuations are stronger in boundary layers. The reason is traced to the extra production in the wake region, and, ultimately, to the irrotational intermittency in that part of the flow.

## INTRODUCTION AND NUMERICAL SCHEME

The purpose of this paper is to present a new simulation of the zero-pressure-gradient turbulent boundary layer in the range  $Re_\theta = 620 - 2140$ , and to compare the results to those of turbulent channels in the same range of Reynolds numbers.

The simulation uses a high-resolution code described in Simens et al. (2009), based on compact finite differences in the streamwise ( $x$ ) and wall-normal ( $y$ ) directions, and on dealiased Fourier expansions along the span ( $z$ ). The longitudinal pressure gradient is controlled by removing fluid through the upper boundary, and is kept very close to zero. Numerical parameters are given in table 1. The turbulent inflow is synthesised by Lund et al's (1998) recycling method, in which the incoming flow is synthesised using data from a downstream reference plane  $x_{ref}$ . Its consequences are carefully investigated, and it is found that the influence of the inflow extends over  $300\theta_0$ , where  $\theta_0$  is the momentum thickness at the inlet. This is almost 25% of the total simulation length and, together with a shorter contaminated region near the outflow, reduces the range of useful Reynolds numbers to  $Re_\theta = 1050 - 2050$  ( $\delta_{99}^+ = 440 - 720$ ).

The reason for this long inflow length can be seen in figure 1(a), which displays the autocorrelation function  $C_{uu}(x; x')$  of a band of spanwise Fourier coefficients of the streamwise velocity, as a function of  $x$ . Besides the primary peak at  $x = x' \approx 1100\theta_0$ , there is a secondary one at  $x = x' - x_{ref} \approx 150\theta_0$ . Lund's method can be interpreted as a physical experiment in which eddies at the reference plane are approximately (except for rescaling) copied to a different position in the boundary layer (the inflow), and allowed to

Table 1: Parameters of the boundary layer simulation.  $L_x$ ,  $L_y$  and  $L_z$  are the box dimensions along the three axes.  $N_x$ ,  $N_y$  and  $N_z$  are the corresponding grid sizes, expressed for  $z$  in terms of collocation points. The resolution is kept of the order of 4 – 6 wall units in the wall-parallel directions, and at least 1.5 Kolmogorov lengths in  $y$ .

$Re_\theta$	$(L_x, L_y, L_z)/\theta_0$	$N_x, N_y, N_z$
620–2140	$1190 \times 64 \times 195$	$6145 \times 360 \times 1536$

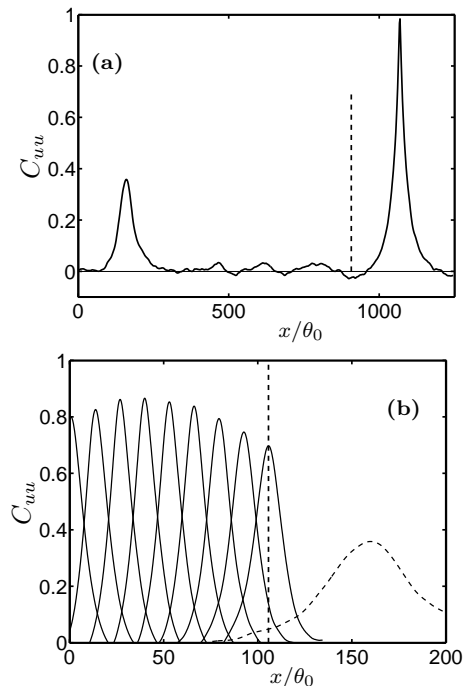


Figure 1: (a) Correlation  $C_{uu}(x; x')$  of the streamwise velocity, as a function of  $x$ . (b) Secondary peaks of  $C_{uu}$ , for various positions of the primary correlation point  $x'$ . —, from a shorter test simulation; - - -, from the final one. For both simulations the displayed correlations are only computed for a band of spanwise wavenumbers around  $\lambda_z/\delta_{99} = 1.7$ , at  $y/\delta_{99} \approx 0.4$ . The dashed vertical line in (a) is the location of the inflow reference plane for the full simulation. The one in (b) is for the test case.

<sup>1</sup>Corresponding author: jimenez@torroja.dmt.upm.es

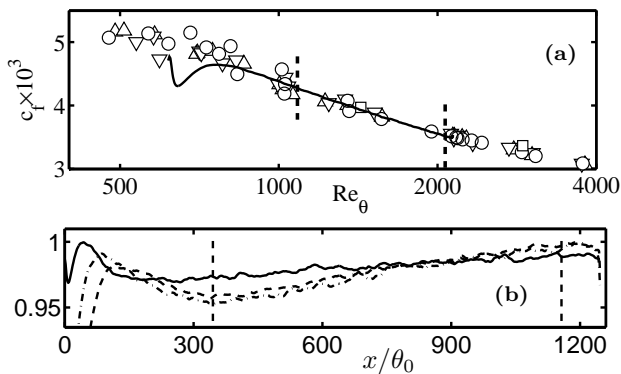


Figure 2: (a) Friction coefficient versus Reynolds number. Open symbols are experiments in Erm and Joubert (1991);  $\square$ , experiments by deGraaff and Eaton (2000); —, present simulation. (b) Peak value of the three velocity-fluctuation intensities, normalised to a common level for the purpose of presentation. —,  $u'$ ; ---,  $v'$ ; - · -,  $w'$ . The dashed vertical lines are the limits of the ‘useful’ range.

evolve. The correlation between the reference and the inflow planes is always large, because one is almost a copy of the other. When the correlation is computed with respect to some location downstream of the reference plane, it reflects, besides the local structure of the eddies, the correspondence between eddies that have been advected from the reference and from the inflow planes. This is the origin of the secondary peak in Fig. 1(a), and its decay with  $x' - x_{ref}$  is a measure of the Lagrangian decorrelation time of the eddies as they are advected by the mean velocity. Both the range of spanwise wavenumbers in figure 1, and the  $y$  location of the correlations, have been chosen to maximize the amplitude of the secondary peak. It is interesting that they correspond to spanwise wavelengths of the order of  $\lambda_z/\delta_{99,ref} \approx 1.5$ , which is somewhat wider than, but of the same order as, the large-scale structures identified in this region of experimental boundary layers by Tomkins and Adrian (2005).

The decay of the secondary peak as it moves away from the inflow is shown in figure 1(b) for a shorter test simulation, and is exceedingly slow. In this case, the reference plane is much closer to the inflow than in the final simulation, and the secondary peak has decayed very little by the time it reaches it. A secondary peak from the final simulation, in which the correlation of the inflow with the reference plane is presumably lower than in the test case, because of the larger rescaling ratio, is still clearly visible at  $x/\theta_0 \approx 160$ . It is known that the decay of the space-time velocity correlation in boundary layers is much slower when the two points are at ‘optimum’ separations than when they are at the same location, showing that the eddies stay coherent while being advected for much longer distances than their lengths (Favre et al. 1958). Figure 1(b) suggests that eddies would stay coherent for 200 – 300 $\theta$ , which is consistent with the lengths found for the persistence of the tripping influence in Erm and Joubert (1991). The physical reason for this long inflow length is that the turnover time for a large eddy of size  $O(\delta_{99})$ , with internal fluctuations of the order of the friction velocity  $u_\tau$ , is  $\delta_{99}/u_\tau$ , during which time the eddy is advected by about  $U_\infty \delta_{99}/u_\tau$ . The implied accommodation lengths, of order  $U_\infty^+ \delta_{99}$ , are consistent with the values found above.

The practical consequence from the point of view of numerical inflow conditions is that the first few hundred momentum thicknesses of a boundary layer are controlled

by the inflow, and that they cannot be used to investigate the structure of turbulence. Better inflow fields may be useful to create more realistic flows, which could for example be used to investigate the effects of turbulence on some other aspect of the flow, but when the physics of the turbulence itself is what is being investigated, the first few hundred momentum thicknesses essentially reflect the hypotheses made for the inflow conditions. Note that this is a problem of any inflow, not only of the recycling method, and that the inflow length estimated here would have to be added to any other length contaminated by local numerical manipulations (e.g., fringes).

The effect of the inflow in our simulation is shown in figure 2(a), which displays the development of the friction coefficient of the simulation,  $2/U_\infty^{+2}$ , as a function of  $Re_\theta$ . It is compared with the experimental results of deGraaff and Eaton (2000), and with those of Erm and Joubert (1991), which cover roughly the same range of Reynolds numbers. The latter are significant because they were designed to test the effect of the tripping, which is probably comparable to the effect of the numerical inflow. All their measurements were repeated with three different tripping devices, which are plotted in figure 2(a) using different symbols. The result was that the effect of the trip survives up to  $Re_\theta \approx 1500$ , and only becomes small beyond that limit. It is seen in figure 2(a) that the same is true in our results, which initially diverge widely from the experiments, but eventually settle into excellent agreement with them at about the same location at which the experimental scatter begins to decrease.

Figure 2(b) presents the evolution of the maxima of the three velocity fluctuations intensities, normalized to a common level for display purposes, and shows even more clearly the effect of the inflow. Following the previous discussion, and the results in these figures, the useful limits of the simulation are chosen to be the vertical dashed lines in figures 2(a) and 2(b), although the experimental tripping results suggest that even the first half of that range may retain some residual inflow effects.

### BASIC STATISTICS

Figure 3 presents streamwise mean velocity and fluctuation intensities near the centre of the computational domain. Also included are the closest available experimental Reynolds numbers from Erm and Joubert (1991), and the simulation by Spalart (1988) at a roughly similar Reynolds number. The agreement is excellent, especially with the experiments.

The figure also includes data from a turbulent channel from del Álamo and Jiménez (2003), and the agreement is reasonable, except for the well-known weaker wake component of the mean velocity profile of the channel. It is unclear how to match Reynolds numbers between boundary layers and channels. Jiménez and Hoyas (2008) concluded that a reasonable choice was to use  $\delta_{99}$  for boundary layers, and the half-width for channels. We will do the same here, and we will loosely refer to both quantities as  $\delta$ . For example, for the boundary layer and channel simulations in figure 3(b), the two Reynolds numbers are  $\delta_{99}^+ = 580$  and  $\delta^+ = 550$ .

The agreement in figure 3 does not hold for the spanwise velocities in figure 4(a), or for the wall-normal velocities (not shown). Neither does it hold for the pressure fluctuations in figures 4(b-c), all of which are stronger in the boundary layer than in the channel. This was already noted by Jiménez and Hoyas (2008) on the basis of incomplete experimental data, and could perhaps be interpreted

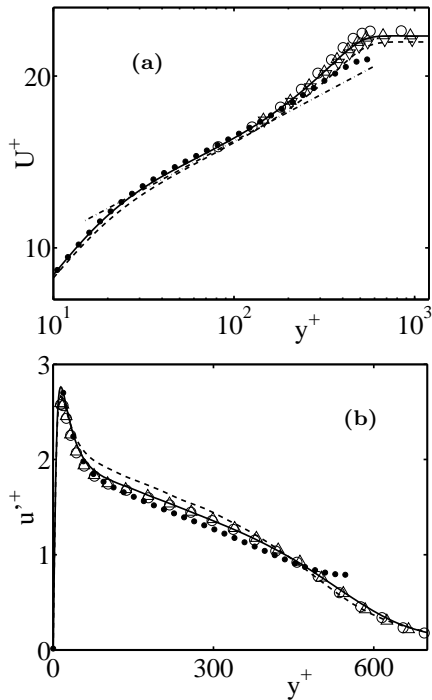


Figure 3: (a) Mean streamwise velocity. —, present simulation at  $Re_\theta = 1350$ ; ---, simulation in Spalart (1988) at  $Re_\theta = 1410$ . Open symbols are as in figure 2,  $Re_\theta \approx 1350$ . •, numerical channel from del Álamo and Jiménez (2003),  $\delta^+ = 550$ ; - - - ,  $\log(y^+)/0.41 + 5$ . (b) Root-mean-squared streamwise velocity. Symbols as in (a), but  $Re_\theta \approx 1550$  ( $\delta^+_{99} \approx 580$ ), both for Erm and Joubert (1991) and for the present simulation.

as that the reference length for boundary layers should be taken larger than  $\delta_{99}$ . However, the value needed to match the transverse velocities and pressures near the wall is about  $1.7\delta_{99}$ , which is rather large, and fails completely to match the profiles above the logarithmic layer. This can be seen, for example, in figure 4(a), where the shapes of the profiles of the two types of flows are very different. Using  $1.7\delta_{99}$  as a reference length for the boundary layers also spoils the agreement in figure 3. There is indeed no reason why the same lengthscale should work for all the variables, or across the whole flow. The boundary layer thickness is associated with the outer flow, and the most reasonable interpretation of the results just discussed is the obvious one that the outer flows of boundary layers and channels are intrinsically different.

This raises the question of which is the nature of those differences, and the reason for them.

**INTERMITTENCY**

The main difference between boundary layers and internal flows, such as channels, is the presence of an irrotational free stream in the former, and the consequent formation of an intermittent layer. Intermittency is used in this paper in the original sense of the large-scale coexistence of irrotational and rotational fluid near the edge of the turbulent region (see for example Kovaszny et al. 1970). In particular, we will define the intermittency coefficient,  $\gamma$ , as the fraction of time that the flow is rotational at a given distance from the wall. This quantity was popular in the early days of boundary layer research, and continues to be used extensively in

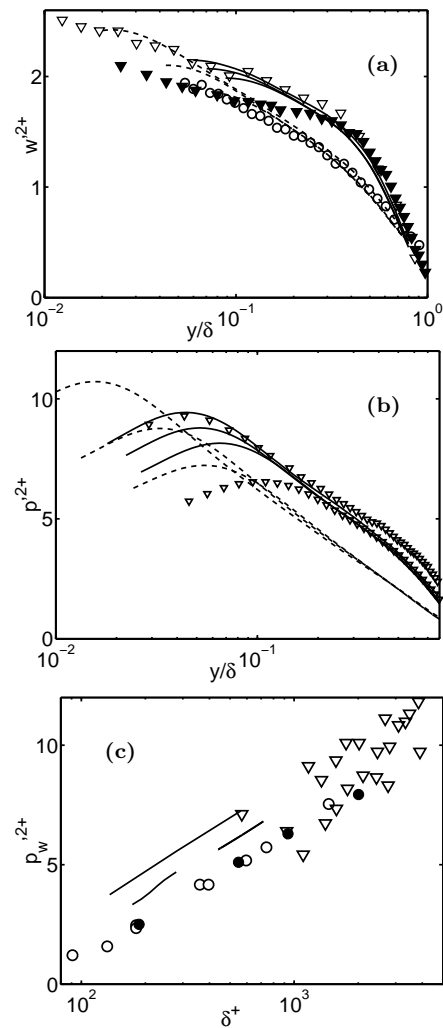


Figure 4: (a) Spanwise velocity fluctuation intensity. (b) Pressure fluctuation intensity. (c) Pressure fluctuation intensity at the wall vs. Reynolds number. Solid lines (numerics) and triangles (experiments) are boundary layers, and dashed lines and circles are channels and pipes. Various sources. Experimental Reynolds numbers are up to  $\delta^+_{99} = 7000$  in boundary layers, and up to  $\delta^+ = 3000$  in channels.

turbulence modelling, because the irrotational fluid influences strongly the flow behaviour. Note that, unfortunately, the same name has later been used for the completely unrelated concept of ‘internal’ intermittency, which refers to the occurrence of occasional large velocity gradients. The measurement of intermittency was difficult in early laboratory experiments because it required the arbitrary estimation, from one-dimensional velocity signals, of whether the flow was irregular enough to be considered turbulent. In simulations it can be made more precise, because the vorticity magnitude  $|\omega|$  can be computed, and irrotational flow can be defined as those points at which the vorticity vanishes. Instantaneous fields of the total vorticity of the boundary layer show irrotational fluid patches that extend well inside the turbulent region. If the probability density function (p.d.f.) of  $|\omega|$  is computed as a function of the wall distance, as in figure 5(a), those patches appear as a delta function at  $|\omega| = 0$ , and the probability contained in it is  $1 - \gamma$ . The results are plotted in figure 5(b), compared with older experimental val-

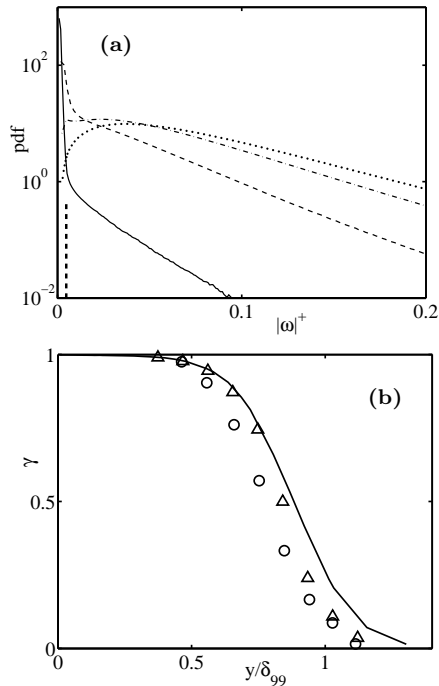


Figure 5: (a) Probability density functions of the vorticity magnitude in the boundary layer,  $Re_\theta = 1550$ , showing the development of the irrotational delta at  $|\omega| \approx 0$ . ..... ,  $y/\delta_{99} = 0.44$ ; -·-·-, 0.59; ---, 0.88; —, 1.31. The dashed vertical line is the limit used to define irrotational flow, slightly larger than a single histogram bin. (b) Intermittency factor. The solid line is the present simulation. o, from experimental velocity measurements,  $Re_\theta = 3000$  (Kovaszny et al. 1970); Δ, from temperature measurements,  $Re_\theta = 1100 - 4800$  (Murlis et al. 1982).

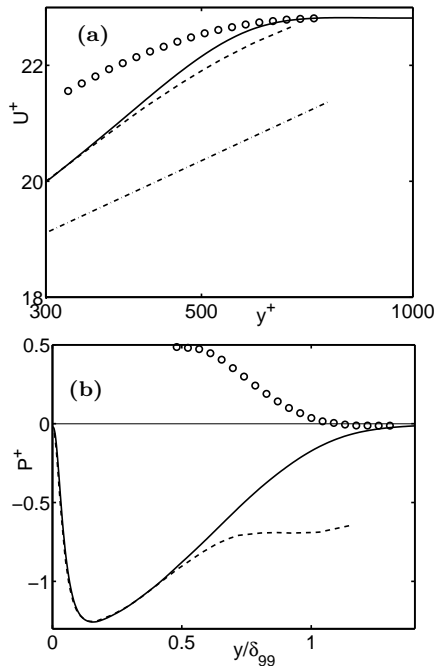


Figure 6: Conditional statistics from present simulation ( $Re_\theta = 1550$ ). —, unconditional average; o, irrotational; ---, rotational. (a) Mean streamwise velocity; the chain-dotted line is  $\log(y^+)/0.41 + 5.2$ . (b) Mean pressure.

ues. The agreement is excellent, considering the differences in Reynolds numbers and in identification techniques, and shows that the irrotational fractions begins to be substantial above  $y \approx \delta_{99}/2$ . It dominates the flow for  $y \gtrsim \delta_{99}$ .

The effect of the intermittency on the mean flow quantities can be studied by means of two-dimensional p.d.f.s of the different variables with  $|\omega|$ , which allow us to compute statistics conditioned to potential or rotational fluid. An example is given in figure 6(a) which shows that the mean velocity is much higher in the potential regions than in the rotational one. This makes sense, because the potential flow has to come from the free stream and, in the absence of turbulence, can only be slowed down by large-scale pressure gradients.

The high velocity of the irrotational regions is interesting, because it provides a plausible explanation for why the high-speed ‘wake’ component of the outer flow is stronger in boundary layers than in internal flows, which are not intermittent. In fact, it is easy to construct plausible arguments for why intermittency should create steeper velocity profiles. Consider a rough model in which the eddy viscosity is determined by the properties of the turbulence, such as the friction velocity and the size  $\delta$  of the largest eddies, and vanishes in the irrotational part. The tangential Reynolds stress, which is fixed by the global momentum balance, has to be carried by the turbulent fraction  $\gamma$ , so that the velocity gradient in the turbulent regions has to increase by  $1/\gamma$ . By itself, this would not change the mean velocity gradient, because it only contributes to a fraction  $\gamma$  of the overall mean velocity gradient. But there is also some velocity gradient in the irrotational part, as seen in figure 6(a), and the result is a net increase of the overall gradient over its non-intermittent value,

$$\partial_y U_{inter} = \gamma \gamma^{-1} \partial_y U_{non-inter} + (1 - \gamma) \partial_y U_{pot}. \quad (1)$$

As we have already mentioned, the only possible interaction between turbulent and irrotational fluid, and therefore the only way to create irrotational velocity gradients, is through the pressure. Its conditional averages are shown in figure 6(b). The pressure in the potential flow is higher than in the free stream, while that in the rotational one is lower, and one could think of the incoming fast potential flow as pushing into the slower rotational fluid ahead of it, while pulling from the one behind. Closer inspection of the conditional p.d.f.s of the pressure reveals that the interaction is more complicated (figure 7a). The cores of the rotational and irrotational distributions are very similar, and the reason for the lower mean pressure in the turbulent regions is that the potential p.d.f.s lack the strong negative tail characteristic of turbulent distributions, usually associated with the vortex cores. The positive pressure associated with irrotational strain behaves almost identically in both regimes.

It is interesting that the pressure fluctuation profiles in figure 4(b) are roughly parallel in the boundary layers and in the channels, and that their offset is due mostly to the faster rise of the fluctuations across the intermittent layer of the boundary layer. Pressure is a global quantity, especially when due to spatially extended sources (Jiménez and Hoyas 2008), and it is tempting to identify the extra pressure fluctuations as coming from the intermittent layer. It is seen in figure 7(b) that the difference between boundary layers and channels is also due to a weaker low-pressure tail in the latter. This suggests that at least part of the vorticity in the boundary layer is organised into structures that are large enough for their effect to be felt across the whole flow thickness. It is again tempting to relate those structures to the

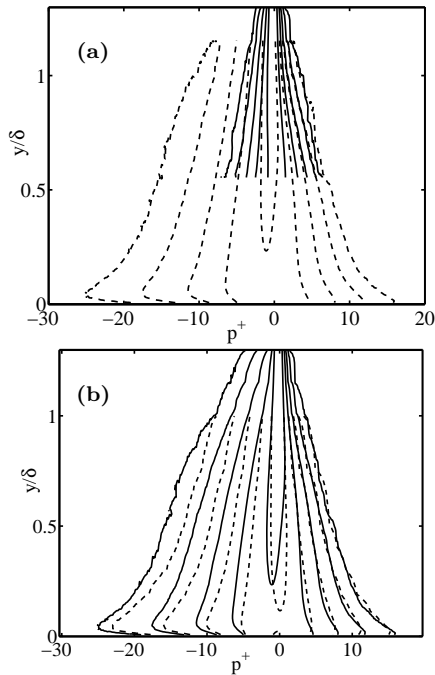


Figure 7: Conditional p.d.f.s of the pressure as a function of the wall distance. (a) —, potential flow; ---, rotational. Boundary layer at  $\delta_{99}^+ = 580$ . (b) Unconditional pressure p.d.f. —, boundary layer; ---, channel at  $\delta^+ = 550$ .

interfacial ramps and bulges mentioned by several authors, and to speculate that they create stronger pressure fluctuations in the boundary layer because they are interspersed with the irrotational patches, but their true nature is still uncertain, and continues to be the subject of investigation. Other p.d.f.s, such as those of the velocities, differ too little from those in channels at these Reynolds numbers to draw useful conclusions.

**ENERGY BALANCES**

The previous discussion can be put in terms of energy fluxes, giving some extra insight into the dynamics involved. The production of the streamwise velocity fluctuations  $P_{uu} = \tau_{xy} \partial_y U$ , where  $\tau_{xy}$  is the Reynolds shear stress, is given in figure 8(a). It is compared with the same quantity from the  $\delta^+ = 550$  channel (Hoyas and Jiménez 2008). This is, of course, the full energy production term, part of which gets redistributed to the transverse velocities by the pressure term  $\Pi_{uu} = \overline{u \partial_x p}$ , which is also given in the figure. Note that the energy budgets have been pre-multiplied by  $y$  to emphasize their behaviours in the outer layers.

It is clear that both the production and the pressure term are larger in the boundary layer than in the channel, which helps to explain why the pressure and the transverse velocities are also stronger. Since pressure preserves continuity, it is not surprising that a by-product of its role in homogenising the differences between the streamwise velocities of the turbulent and potential regions should be to enhance the transverse fluctuations.

The two factors in the energy production are shown independently in figures 8(b) and 8(c). They show that the main reason for the larger production in the boundary layers is the steeper velocity gradient, which is the same thing as

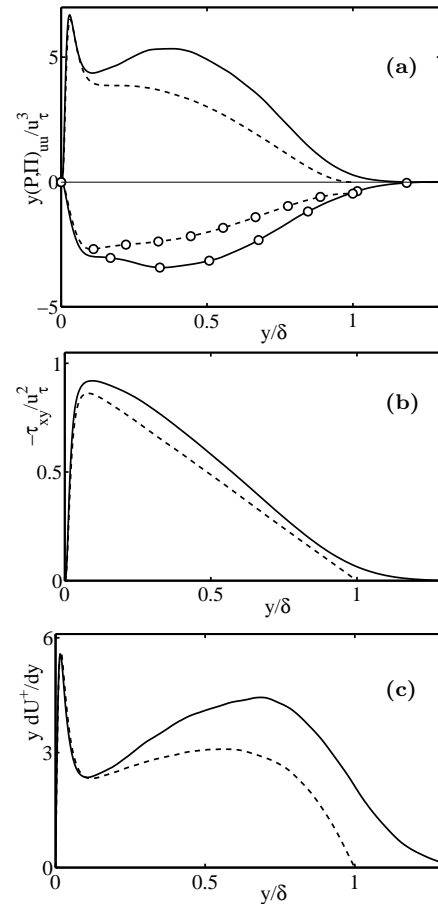


Figure 8: Energy budgets for the streamwise velocity fluctuations. —, present boundary layer,  $\delta_{99}^+ = 580$ ; ---, channel,  $\delta^+ = 550$ . (a) Lines without symbols are the production,  $\tau_{xy} \partial_y U$ , and those with symbols are the pressure-redistribution term towards the two other velocity components. Note that the curves are pre-multiplied by  $y$ , to emphasize the outer part. (b) Shear Reynolds stress (c) Pre-multiplied mean velocity gradient.

the wake.

**CONCLUSIONS**

We have presented a new direct simulation of the zero-pressure gradient boundary layer with a useful range  $Re_\theta \approx 1000 - 2000$ . After a long inflow region, caused by the slow evolution of the largest eddies, the results are in excellent agreement with older simulations and with experiments. When they are compared with turbulent channels at similar Reynolds numbers, it is found that even the low order statistics of boundary layers and channels differ considerably, including in some cases the values within the buffer layer.

In general the pressure and the transverse velocity fluctuations are stronger in boundary layers than in channels, while the streamwise fluctuation intensities are roughly similar for both cases. The differences between the two flows are traced to an excess of production of the streamwise turbulent energy in the outer part of the boundary layer, which is about 50% stronger than in the same region of channels. This is mostly associated with the stronger mean velocity gradient in the boundary layers, which is a reflection of the stronger wake component of their velocity profiles.

We have shown that the root of the stronger wake is the intermittent irruption of potential flow in the outer part of the boundary layer, which is absent in the channel. The incoming irrotational flow, lacking the ability to effectively mix momentum, retains the faster velocity of the free stream relatively deep into the boundary layer. The extra velocity gradient in the wake generates a more active production of turbulent energy, most of which is distributed to the transverse components by the pressure-strain term. This is the reason for the stronger pressure fluctuations, and, since they extend to the wall, also explains the observed differences in the transverse velocities.

The differences between the statistics of boundary layers and internal flows are also found in experiments at higher Reynolds numbers (Jiménez and Hoyas 2008), although quantities such as the pressure fluctuations and the energy budgets are not available for them. These results suggest that caution should be exercised when using data from different flows to document, for example, Reynolds number effects in shear turbulence.

This work was supported in part by the CICYT grant TRA2006-08226, by Industria de Turbopropulsores S.A., and by the EU FP6 Wallturb Strep AST4-CT-2005-516008. The computations were made possible by generous grants of computer time from the Barcelona Supercomputing Centre, and by the equally generous use of the mass storage facilities of the Port d'Informació Científica (PIC). MPS was supported in part by the EU FP5 Training and Mobility Network HPRN-CT-2002-00300, and SH and YM by the Juan de la Cierva program of the Spanish Ministry of Education and Science.

## REFERENCES

- Del Álamo, J. C. and Jiménez, J., 2003, "Spectra of very large anisotropic scales in turbulent channels", *Phys. Fluids*, vol. 15, pp. L41–L44.
- DeGraaff, D. B. and Eaton, J. K., 2000, "Reynolds number scaling of the flat-plate turbulent boundary layer", *J. Fluid Mech.*, vol. 422, pp. 319–346.
- Erm, L. P. and Joubert, P. N., 1991, "Low-Reynolds-number turbulent boundary layers", *J. Fluid Mech.*, vol. 230, pp. 1–44.
- Favre, A. J., Gaviglio, J. J., and Dumas, R. J., 1958, "Further space-time correlations of velocity in a turbulent boundary layer", *J. Fluid Mech.*, vol. 3, pp. 344–356.
- Hoyas, S. and Jiménez, J., 2008, "Reynolds number effects on the Reynolds-stress budgets in turbulent channels", *Phys. Fluids*, vol. 20, p. 101511.
- Jiménez, J. and Hoyas, S., 2008, "Turbulent fluctuations above the buffer layer of wall-bounded flows", *J. Fluid Mech.*, vol. 611, pp. 215–236.
- Kovaszny, L., Kibens, V., and Blackwelder, R., 1970, "Large-scale motion in the intermittent region of a turbulent boundary layer", *J. Fluid Mech.*, vol. 548, pp. 283–325.
- Lund, T. S., Wu, X., and Squires, K. D., 1998, "Generation of turbulent inflow data for spatially-developing boundary layer simulations", *J. Computat. Phys.*, vol. 140, pp. 233–258.
- Murlis, J., Tsai, H., and Bradshaw, P., 1982, "The structure of turbulent boundary layers at low Reynolds numbers", *J. Fluid Mech.*, vol. 122, pp. 13–56.
- Simens, M. P., Jiménez, J., Hoyas, S., and Mizuno, Y., 2009, "A high-resolution code for turbulent boundary layers", *J. Computat. Phys.*, doi: 10.1016/j.jcp.2009.02.031.
- Spalart, P. R., 1988, "Direct simulation of a turbulent boundary layer up to  $Re_\theta = 1410$ ", *J. Fluid Mech.*, vol. 187, pp. 61–98.
- Tomkins, C. D. and Adrian, R. J., 2005, "Energetic spanwise modes in the logarithmic layer of a turbulent boundary layer", *J. Fluid Mech.*, vol. 545, pp. 141–162.